ELSEVIER

Materials Science and Engineering A289 (2000) 208–216

MATERIALS SCIENCE & ENGINEERING A

www.elsevier.com/locate/msea

Fatigue crack-growth in shape-memory NiTi and NiTi–TiC composites

R. Vaidyanathan, D.C. Dunand [1], U. Ramamurty *

Department of Materials Science and Engineering, Massachusetts Institute of Technology, Cambridge, MA 02139, USA

Received 4 November 1999; received in revised form 2 March 2000

Abstract

An experimental study was conducted to examine the room-temperature fatigue crack-growth characteristics of shape-memory NiTi matrix composites reinforced with 10 and 20 vol.% of TiC particles. Microstructural characterization of these hot-isostatically-pressed materials shows that the TiC particles do not react with the NiTi matrix and that they lack any texture. Overall fatigue crack-growth characteristics were found to be similar for the unreinforced and reinforced materials. However, a slight increase in the threshold for fatigue crack initiation was noted for the composites. The fracture toughness, as indicated by the failure stress intensity factor range, was found to be similar for all materials. Neutron diffraction studies near the crack-tip of the loaded fracture NiTi specimen detected no significant development of texture at the crack-tip. These results are explained by recourse to fractographic observations. Finally, a comparison is made between the micromechanisms of fracture of metal matrix composites, which deform by dislocation plasticity, and those of the present NiTi–TiC composites, which deform additionally by twinning.

Keywords: Shape memory alloys; Metal matrix composites; Fatigue and fracture; Micromechanisms; Neutron diffraction

1. Introduction

The intermetallic NiTi can exist near room-temperature as a cubic (B2) austenite phase or a monoclinic (B19′) martensite phase. The martensite phase consists of 24 variants with varying crystallographic orientations and can deform by twinning, producing macroscopic tensile strains as high as 8%. Heating results in a phase transformation to the austenite phase and recovery of all the macroscopic strain accumulated by twinning, a phenomenon known as shape-memory. The transformation is thermoelastic and can also be affected by changes in stress, a related phenomenon called superelasticity or pseudoelasticity [1,2].

Dunand and co-workers [3–8] have extensively studied shape-memory NiTi composites reinforced with TiC particles. The choice of TiC as reinforcement was motivated by the lack of reactivity with NiTi, which could otherwise adversely affect the shape-memory characteristics. The NiTi–TiC system's thermal transformation behavior [3,4], bulk mechanical properties in compression [5], and subsequent shape-memory recovery [6], and the study by neutron diffraction of twinning deformation and shape-memory recovery have been investigated [7,8]. More recently, their behavior in tension and two-way shape-memory response (wherein the transformation to martensite on cooling is biased) have been studied [9,10]. These studies show that the TiC reinforcements can be successfully utilized to tailor the mechanical properties of NiTi in a cost-effective manner. However, to date there has been no study on the crack-growth behavior of such composites.

The present work is initiated with the following twin objectives: (a) to study the effect of TiC reinforcement on the fatigue crack growth properties of NiTi shape-memory alloys; and (b) to examine twinning ahead of the crack-tip with neutron diffraction. These objectives were accomplished by experiments on NiTi with 0, 10 and 20% TiC particles.

* Corresponding author. Present address: Department of Metallurgy, Indian Institute of Science, Bangalore 560012, India.

[1] Present address: Department of Materials Science and Engineering, Northwestern University, Evanston, IL 60208, USA.

0921-5093/00/$ - see front matter
PII: S0921-5093(00)00882-0

2. Experimental procedures

2.1. Sample fabrication

Cylindrical billets of the following nominal compositions were fabricated using hot isostatic pressing (HIP): (a) unreinforced NiTi; (b) 10 vol.% TiC in a NiTi matrix; and (c) 20 vol.% TiC in a NiTi matrix. These materials are designated in this paper as NiTi, NiTi–10TiC, and NiTi–20TiC, respectively. Pre-alloyed 99.9% pure NiTi powders (49.4 at.% Ni) with size ranging between 44 and 177 μm (obtained from Special Metals, New York) were used to fabricate the monolithic billet. For the composites, the pre-alloyed powders were blended with 99.9% pure, equiaxed TiC powders of 44 μm average diameter (obtained from Atlantic Equipment Engineers, NJ). The powders were packed in a cylindrical low carbon steel container (thickness 0.318 cm, internal diameter 9.1 cm, length 16.5 cm, lined with a boron nitride coated nickel foil to prevent carbon contamination) and were subjected to HIP at 1065°C under an applied pressure of 100 MPa for 3 h.

The HIP billets were electro-discharge-machined (EDM) to yield compact-tension (CT) test specimens (each 50 by 48 mm and 10 mm thick and sized according to ASTM standard E-399). These monolithic and composite samples were solutionized at 930°C for 1 h under flowing, titanium-getterred, argon and furnace cooled to room temperature.

2.2. Microstructural characterization

The transformation temperatures associated with the start and finish of the transformation during heating (i.e. A_s and A_f) and cooling (i.e. M_s and M_f) were determined using differential scanning calorimetry (DSC). A Perkin Elmer DSC-7 Calorimeter was used at a rate of 1 $K \cdot min^{-1}$ under nitrogen cover gas.

The average grain-size was determined by image analysis of optical micrographs. Electron microprobe (using a JEOL superprobe 733 calibrated with pure Ni and Ti) was used to check the matrix for compositional variations away from a TiC particle. The stoichiometry of the as-received TiC powders was ascertained using combustion analysis (with infrared detection). The densities of the samples used were determined by water-displacement.

Table 1
Transformation temperatures (°C) of shape-memory NiTi, NiTi–10TiC and NiTi–20TiC

Sample	M_f (±2°C)	M_s (±2°C)	A_s (±2°C)	A_f (±2°C)
NiTi	35	49	66	86
NiTi–10TiC	23	40	54	75
NiTi–20TiC	−4	18	25	46

2.3. Mechanical testing

A servo-hydraulic machine operating under load-control was used for crack growth experiments. The NiTi and NiTi–10Ti samples were initially ice-water quenched to make sure that they were completely martensitic (see Table 1). NiTi–20TiC was also ice-water quenched but may not have been fully martensitic, as discussed in a later section. All the samples were tested at room temperature (about 20°C) at a load ratio (defined as the ratio of minimum load to maximum load) $R = 0.1$ with a sinusoidal frequency of 15 Hz. Crack extension was monitored using a long-range Questar telescope system. The specimens were pre-cracked with an applied stress intensity factor range (ΔK) of about 10 $MPa\sqrt{m}$ until the crack reached a length of approximately 1.5 mm. The load shedding technique was then used to obtain a threshold stress intensity factor range. The load was then systematically increased to obtain a failure value.

2.4. Neutron diffraction studies

To confirm that the HIP specimens had no initial texture, neutron diffraction was used. Detailed information on the experimental setup can be found elsewhere [11,12] and is only summarized here. Neutron diffraction measurements were performed in 'time of flight' mode using the neutron powder diffractometer (NPD) at the pulsed neutron source at Los Alamos National Laboratory (LANL). The NiTi sample was placed in the beam and neutron diffraction spectra were acquired in two scattering geometries. The sample axis (normal to the largest face) formed an angle of 45° with the incident neutron beam, allowing measurements for which the scattering vectors were parallel and perpendicular to the sample axis.

For neutron diffraction studies on the nature of deformation ahead of the crack-tip, a precracked NiTi CT specimen (50 by 48 mm and 4 mm thick) was used. The sample set-up was identical to that described in the previous paragraph, with the sample axis (normal to largest face) at 45° to the incident neutron beam, allowing for acquisition of diffraction information from lattice planes perpendicular and parallel to the sample axis. The loading direction was perpendicular to the sample axis. The neutron beam spot size was limited to $\sim 3 \times 3$ mm^2 and measurement times were about 12 h for each spectrum. Five measurements were made. (1) At a spot far from the crack-tip without any applied

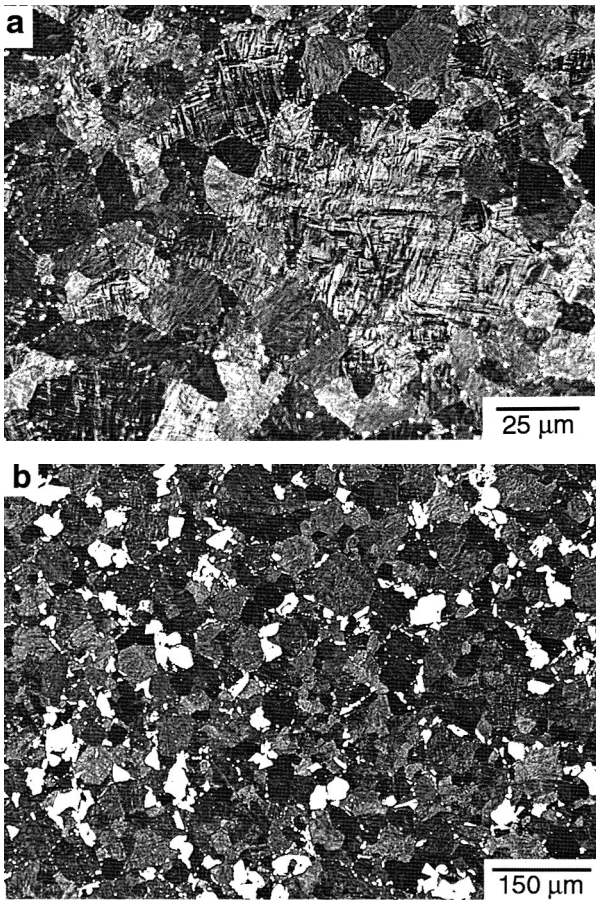

Fig. 1. Optical micrographs of (a) NiTi and (b) NiTi–10TiC.

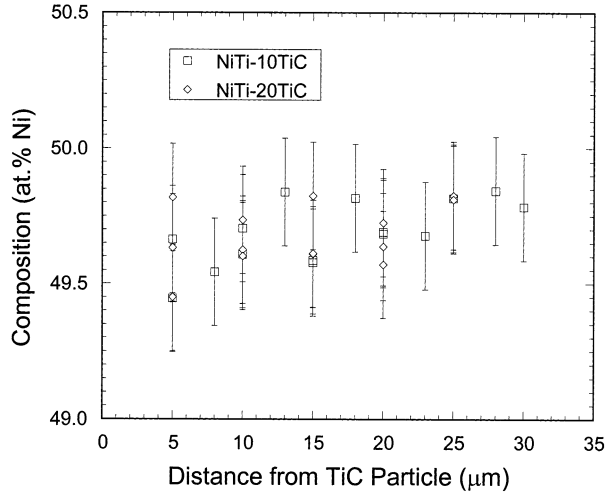

Fig. 2. Microprobe analysis of shape-memory NiTi–10TiC and NiTi–20TiC.

load to represent the undeformed sample. (2) At a spot directly centered ahead of the crack-tip without any applied load. (3) With a static stress intensity $K = 25$ MPa$\sqrt{\text{m}}$ and (4) 32 MPa$\sqrt{\text{m}}$ at the same spot as in (2). (5) With a $K = 32$ MPa$\sqrt{\text{m}}$ at a position 1 mm above the crack tip.

3. Results

The transformation temperatures of NiTi, NiTi–10TiC and NiTi–20TiC are presented in Table 1. These results have also been verified by electrical resistivity measurements on the same ingots in Ref. [9]. From this table, it is seen that the transformation temperatures of NiTi are significantly altered by the addition of TiC particulates, as described in more detail in Refs. [3,4]. Density measurements show that NiTi, NiTi–10TiC, and NiTi–20TiC are 99.8, 99.7, and 99.4%, respectively, of their theoretical density.

Representative micrographs of NiTi and NiTi–10TiC are shown in Fig. 1. The distribution of TiC particles in the composite microstructures was uniform without any agglomeration. The TiC particles were observed to be located at the prior particle boundaries. This is expected given that the starting powders were blended (as opposed to mechanically alloyed) and were of comparable sizes. The average grain-size was determined to be 11 ± 3 μm for NiTi and 13 ± 3 μm for both composites. The results of the microprobe analysis away from a TiC particle are plotted in Fig. 2. The TiC particles were almost stoichiometric with a composition of 49.8 ± 0.1 at.% C. No third phases have been reported in the NiTi–TiC system over a large range of compositions [13,14]. The unreacted interfaces observed with the aid of optical microscopy in the samples confirm that the TiC particles behaved as chemically inert reinforcements. Fig. 2 also shows no change in atomic composition of the matrix as a function of distance from a TiC particle, indicating that interdiffusion is negligible. The lack of large-scale interdiffusion between NiTi and TiC cannot be taken for granted if TiC is non-stoichiometric [15]. Hence the combustion analysis result from TiC (i.e. of negligible deviations from stoichiometry) is consistent with the observations from the microprobe analysis.

Fig. 3 shows neutron diffraction spectra obtained from detectors that were perpendicular to each other. In cases where there is no texture in the diffracting volume, spectra from two such detectors would be expected to be similar. The very close concurrence between the spectra obtained from two perpendicular detectors (Fig. 3) indicates that the martensite is untextured. The texture in the samples was quantified using a spherical harmonic description of the texture [16,17] in a Rietveld refinement [18]. The Los Alamos National Laboratory code, General Structure and Analysis System (GSAS) [19] was used for the refinement. Martensitic NiTi was determined to have no initial texture in the bulk and a texture index [16] of $J = 1.030$ was observed (unity corresponds to a polycrystal with randomly orientated grains and infinity to an ideal single crystal).

Tensile test results obtained on materials from the same ingots and reported in Refs. [9,10] are reproduced in Fig. 4. These tests were conducted at an initial tensile strain rate of 0.05 min^{-1} in a controlled temperature environment at a temperature of 15°C below M_f (i.e. with fully martensitic samples). After an initial quasi-elastic region, twinning for NiTi starts near 100 MPa (twinning yield stress) and finishes near 300 MPa, leading to a plateau. Further loading leads to elastic deformation of the fully twinned martensite, followed by yielding due to dislocation plasticity at about 700 MPa (slip yield stress) and strain-hardening up to the failure stress of 950 MPa. From Fig. 4, it can also be seen that the twinning yield stress increases with increasing TiC content, while the slip yield stress decreases with increasing TiC content. A significant reduction in the ductility is observed from 21% for NiTi to 8% for NiTi–10TiC to 5% for NiTi–20TiC.

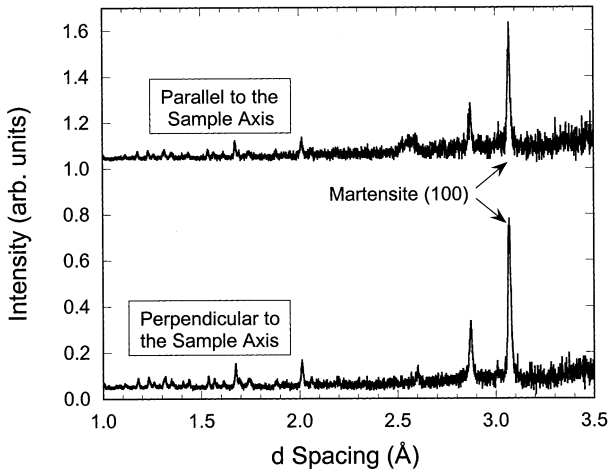

Fig. 3. Neutron diffraction spectra of NiTi fabricated by hot isostatic pressing (HIP). Spectra are shown for lattice planes diffracting parallel and perpendicular to the sample axis.

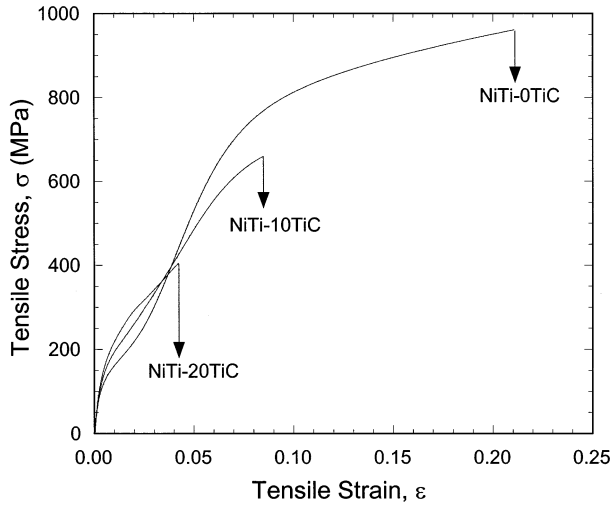

Fig. 4. Tensile stress–strain response of shape-memory NiTi, NiTi–10TiC and NiTi–20TiC at 15°C below the M_f (from [9]).

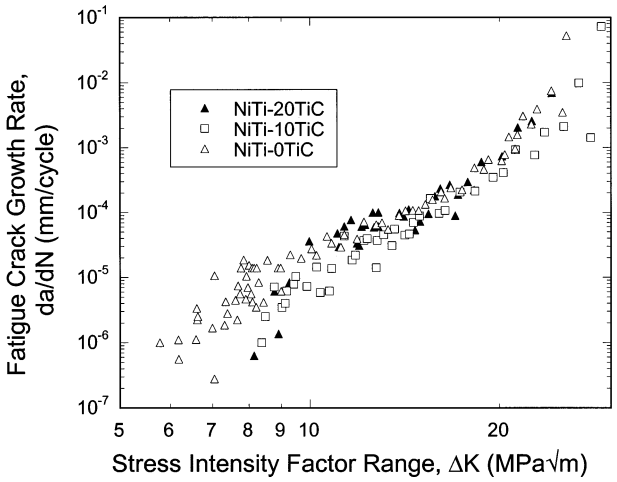

Fig. 5. Fatigue crack growth rate, da/dN, vs. stress intensity factor range, ΔK, curves for shape-memory NiTi, NiTi–10TiC and NiTi–20TiC at room temperature.

Table 2
Results of fatigue-crack growth experiments at room temperature for shape-memory NiTi, NiTi–10TiC and NiTi–20TiC

Sample	Stress intensity factor range ΔK (MPa$\sqrt{m}$)		Paris exponent
	Threshold	Failure	
NiTi	5.8	25.5	4.5
NiTi–10TiC	8.4	29	6.1
NiTi–20TiC	8.1	24.2	5.2

Fig. 5 shows the fatigue crack growth behavior of the composites where the crack growth rate, da/dN, is plotted against the stress intensity factor range, ΔK. The crack growth curves exhibit the classical features of well-defined threshold, steady-state (Paris regime) and final failure regimes. The threshold stress intensity factor range, ΔK_0, for the unreinforced material (5.8 MPa$\sqrt{m}$) is similar to that ($\sim$5 MPa$\sqrt{m}$) reported by Dauskardt et al. [20] for a near-equiatomic NiTi alloy with a stable martensitic structure. However, it is significantly larger than that reported ($\sim$3.2 MPa$\sqrt{m}$) by Holtz et al. [21] for a hot rolled, near-equiatomic NiTi alloy with a M_s of 80°C. The ΔK_0 increases by about a third with the addition of TiC to NiTi (Table 2). The intermediate regime of fatigue crack growth can be fitted with the Paris law [22]:

$$\frac{da}{dN} = C\Delta K^m \quad (1)$$

where C and m are material constants. The Paris exponent m and the threshold and failure stress intensity factor ranges are listed in Table 2. It is seen that the m value for the unreinforced martensitic NiTi ($\sim$4.5) is

slightly higher than that (~ 3.5) inferred from the data reported by Dauskardt et al. [20] and Holtz et al. [21] on similar materials.

4. Discussion

Prior to discussing the crack growth results, it is necessary to emphasize the significant influence of initial texture on the properties of NiTi [23]. Before the onset of plastic deformation through dislocation motion, martensite deforms by twinning wherein some favorably oriented martensite variants reorient or grow at the expense of less-favorably oriented ones [1]. Hence, initial texture has a major effect on the mechanical response of martensitic NiTi. The motivation for fabricating all our materials in an identical manner by HIP was to obtain texture-free samples and thus measure intrinsic NiTi properties. Both neutron and X-ray diffraction can be used to quantify texture. However, the former technique has a penetration of several millimeters providing a bulk measurement (averaged over several grains), while the latter technique can be used to probe only a thin layer near the surface owing to the limited penetration depth of X-rays. Since the incident neutron beam is polychromatic, information from crystallographic planes parallel or perpendicular to the loading direction can be obtained by choosing data from the appropriate detectors. The near exact concurrence between the spectra obtained from two perpendicular detectors (Fig. 4) confirms that the martensite is not textured, as expected from the HIP procedure. This can be contrasted with stress-induced martensite that is highly textured (wherein the (100) peak is visible in one detector and absent in another detector [24]), and with martensitic samples produced after cooling of austenitic samples which had been rolled or drawn.

The texture index of 1.030 also confirms the lack of preferred orientation in the NiTi. Eshelby's inclusion theory was used to determine the residual stress due to the thermal expansion mismatch between the matrix and TiC [25,26]. The matrix has a mean tensile stress of 26 and 51 MPa (for NiTi–10TiC and NiTi–20TiC, respectively) due to this mismatch. This low stress cannot be expected to cause significant twinning in the matrix of the composites that are consequently expected to also be texture-free.

The crack-growth properties of monolithic NiTi have previously been investigated [20,21,27]. Earlier work by Melton and Mercier [27] shows that the ΔK_0 is sensitive to the M_s, decreasing with increasing M_s, while the crack growth rates in the Paris regime are unaffected by M_s. Dauskardt et al. [20], with their experimental work on non-transforming and transforming NiTi alloys, have shown that the fatigue crack growth rates were much slower in non-transforming microstructures. They attribute the decreased crack growth resistance in NiTi with a transforming microstructure to lowered crack-tip shielding which arises from negative, but small, dilatation strains associated with the austenite-to-martensite transformation. Holtz et al. [21] have studied the fatigue crack growth behavior of a NiTi alloy with a M_s of 80°C in both vacuum and air and under different load-ratios with the primary focus on the near-threshold behavior. For a load-ratio of 0.1, the fatigue threshold in vacuum was observed to be significantly higher (by $\sim 200\%$) than that observed in air. On the basis of their experimental observations, Holtz et al. [21] conclude that the near-threshold fatigue crack growth behavior is influenced by two competing fatigue mechanisms and suggest that at low ΔK, atmospheric environmental interactions associated with microstructural processes dominated by martensite twin variants are operative whereas at high ΔK, grain-boundary dominated fatigue mechanisms are dominant.

As noted in the previous section, the fatigue threshold and the Paris exponent for the unreinforced alloy observed in the present study are different from those reported in the literature for similar NiTi materials [20,21]. The differences in the M_s could be one of the possible reasons for these differences, as inferred from the work of Melton and Mercier [27]. The other possible reason is the presumed presence of texture (due to hot rolling) in the material studied by Holtz et al. [21].

In contrast to the previous studies mentioned above, the focus of the present work is to compare the fatigue crack growth behavior of the composites with that of the unreinforced alloy. From Table 1, it can be inferred that both NiTi and NiTi–10TiC samples, when tested at room temperature after an ice-water quench, are fully martensitic. Given the comparable densities (the small difference is attributed to porosity in TiC), grain sizes and the lack of interfacial reaction between NiTi and TiC, the crack-growth behavior of NiTi and NiTi–10 TiC can be directly compared. However, the NiTi–20TiC composite has a transformation temperature $M_f = -4$°C, indicating that small quantities of austenite are probably retained in this sample after quenching. Also, with $A_s = 25$°C, further formation of austenite may have occurred at room temperature under the crack growth experimental conditions. While the volume fraction of austenite was probably small in NiTi–20TiC, the results obtained from this material may not be directly comparable with those of the fully martensitic NiTi and NiTi–10TiC specimens. Indeed, the smaller value of the Paris exponent, m, in NiTi–20TiC as compared to NiTi–10TiC (Table 2) may be due to the presence of small quantities of austenite in the former material, which may increase crack tortuosity. Also, the higher Paris exponents found in the composites as compared to monolithic NiTi are expected, given the higher tensile ductility of the latter material.

The failure stress intensity factor range, ΔK_f, varies only marginally in the composites as compared to unreinforced NiTi (Table 2). This observation indicates that the fracture toughness, K_{Ic} ($=\Delta K_f/(1-R)$), is not affected significantly by the addition of TiC to NiTi.

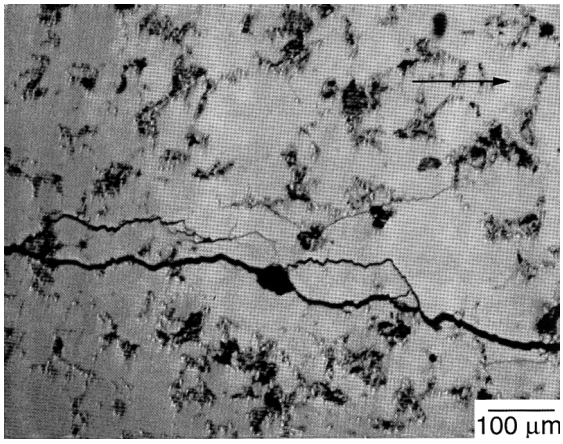

Fig. 6. An optical micrograph showing the tortuous nature of fatigue crack growth in NiTi–10TiC due to the TiC particles. Arrow indicates the crack growth direction.

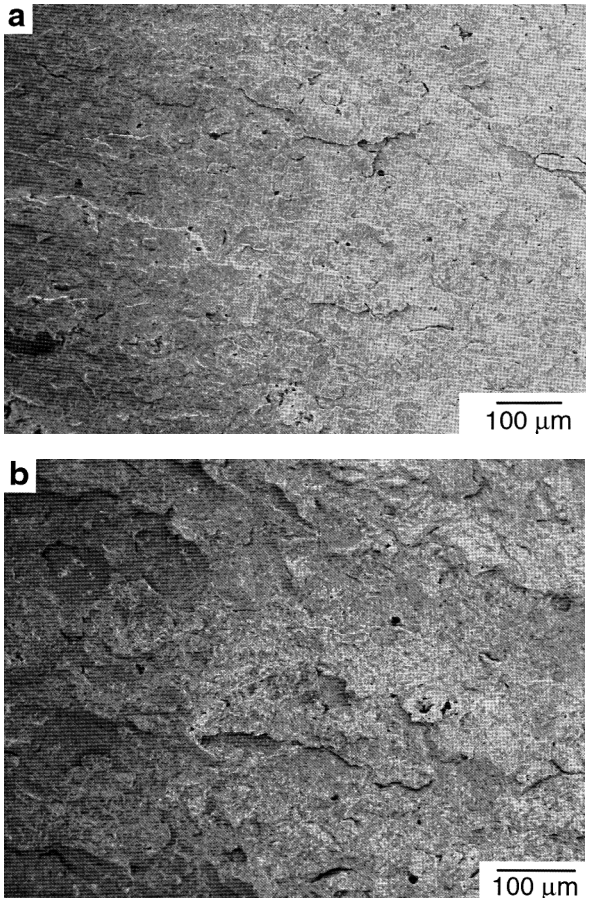

Fig. 7. Low magnification SEM micrographs of the fractured specimens showing (a) a relatively flat fracture plane in NiTi and (b) a rough fracture surface in the NiTi–10TiC.

However, the tensile tests show the composites to be more brittle than NiTi, from which a lower K_{Ic} would be expected for the composites. This observation holds even if NiTi–20TiC is ignored because of its slightly different microstructure. A possible explanation for this discrepancy could be that the TiC particles are acting as fracture initiation sites during the plastic deformation at high strains for the unnotched tensile specimens. However, because of the already high strains at the crack-tip regions in the fracture specimens, their adverse effect is not reflected in the fracture toughness data.

Another possible reason for similar values of fracture toughness in all the materials studied could be the promotion of crack-deflection by the TiC particles in the case of composites. Fig. 6 is an optical micrograph showing evidence of crack deflection in the fracture path of the NiTi–10TiC CT specimen. Fractographic observations also indicate a similar scenario. Low magnification SEM micrographs of the fractured NiTi and NiTi–10TiC specimens are shown in Fig. 7a and b, respectively. Fig. 8a–c show the fatigue fracture regime, fast fracture regime, and intergranular cracking in the fatigue cracked area for NiTi, respectively. It is seen from these figures that, on a macroscopic level, the fracture plane appears to be relatively smooth for the NiTi (Fig. 7a) whereas it is considerably rougher for the composite (Fig. 7b). Thus, crack deflection is aided by the TiC particles that reduce the crack-tip stress intensity factor and hence lead to higher fracture toughness values.

Previous work on fatigue crack growth in NiTi shape-memory alloys [28] has demonstrated that the crack propagation rate is insensitive to the test temperature below the start of the martensite transformation (M_s). Since NiTi and NiTi–10TiC both were tested below M_s, it is likely that the matrix is dominating and the particles do not significantly influence the crack growth behavior in the composites. It has been established that in the case of shape-memory [8] and superelastic composites [12,25] the mismatch between reinforcement and matrix (thermal, elastic and allotropic) is largely accommodated. Hence given the low volume fraction of TiC and the accommodation of the mismatch it is understandable that both NiTi and NiTi–10TiC exhibit similar crack-growth behavior.

Closer examination of the fracture surfaces with SEM reveals additional features. For NiTi, the features in the fatigue fracture region have smooth step patterns with cleavage-like features (Fig. 8a). In contrast, the fast fracture regime in NiTi shows a more dimple-like fracture morphology (Fig. 8b). It is interesting to note that both the fatigue and fast fracture features are distinctly similar to those observed in Ti alloys that also deform through extensive twinning [29]. Some intergranular cracking was also observed in NiTi (Fig. 8c)

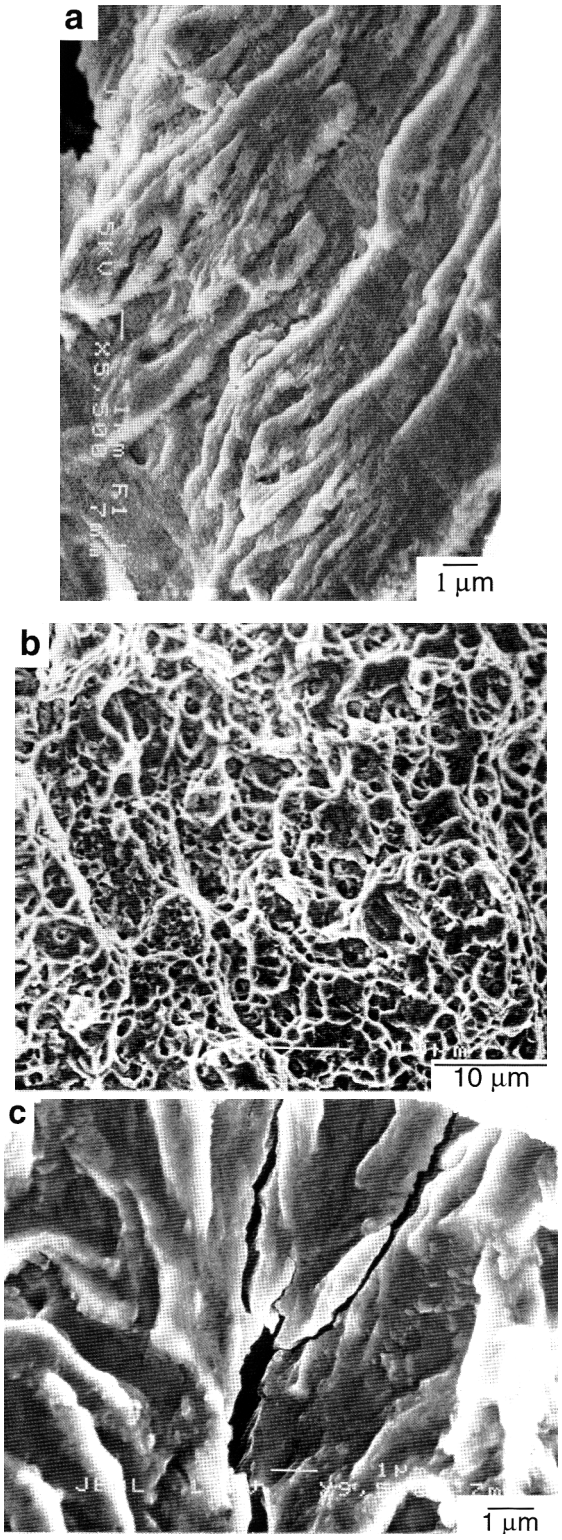

Fig. 8. Fractographic observations on the fatigue fractured NiTi specimen. (a) Fatigue fracture regime, (b) fast fracture regime, and (c) intergranular cracking in the fatigue cracked area.

which could possibly be due to the strain incompatibility between various grains.

Fracture features on TiC reinforced composite, on the other hand, are markedly different. In the fatigue-cracked area, the matrix features are cleavage-like and clear debonding between matrix and precipitates is noticeable (Fig. 9a). Extensive microcracking, which appears to be aided by the fracturing of reinforcement particles, is also observed (Fig. 9a and b) an In the fast-fracture regime, only debonding accompanied by matrix ductile fracture features is observed but no particle fracture was noted (Fig. 9c). The fractographic observations suggest that microcracking due to particle

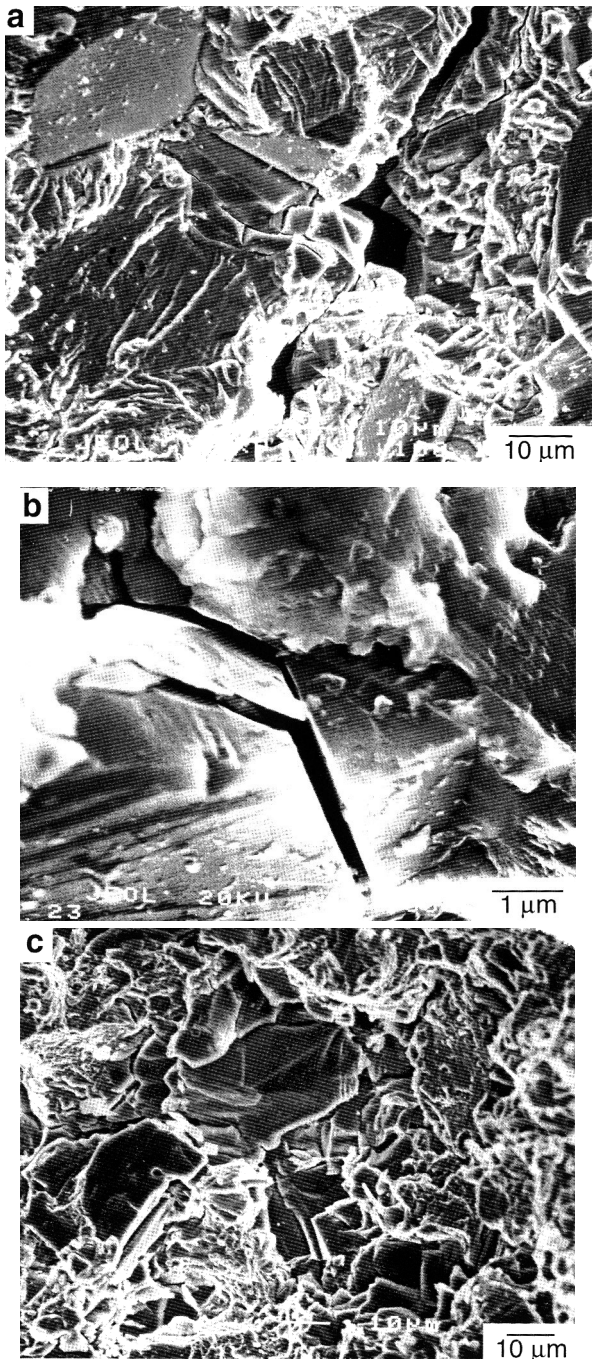

Fig. 9. Fractographic observations on the fatigue fractured NiTi–10TiC specimen. (a) Fatigue cracked area, (b) TiC particle fracture in the fatigue cracked area, and (c) fast fracture regime.

Table 3
Texture indices of martensitic NiTi from neutron diffraction data

Location	Texture index J
Far from crack-tip	1.030
Crack-tip (no load)	1.023
Crack-tip ($K = 25$ MPa$\sqrt{\text{m}}$)	1.030
Crack-tip ($K = 32$ MPa$\sqrt{\text{m}}$)	1.051
Off crack-tip ($K = 32$ MPa$\sqrt{\text{m}}$)	1.023

fracture could be a crack-tip shielding mechanism that leads to higher crack growth resistance. Microcracking may arise due to the large stain incompatibility between the strains in the NiTi and the TiC.

The results of the neutron diffraction measurements on the NiTi precracked specimen are presented in Table 3 after Rietveld refinements. The stress intensity or position with respect to the crack tip does not affect the texture index (within experimental error). The texture index is very close to unity and thus very low compared to values as high as 6 that have been reported for stress-induced martensite [12]. The lack of significant changes in texture is somewhat surprising. A conservative estimate of the twin zone size at the crack-tip, $r_p \approx 0.1(K_I/\sigma_y)$, where σ_y is the twinning yield stress for martensite, shows that the neutron beam size (3 mm) is smaller than the twin zone size (~ 4.25 mm). Hence, the texture due to extensive deformation at the crack-tip should be measurable. The absence of significant texture is possibly due to macro-averaging which occurs because of the large volume of sampling (~ 25 mm^3) and because of the symmetric nature of twinned structures. It is also possible that significant texture is inhibited by dislocation plasticity ahead of the crack-tip and the multi-axial state of stress. Further investigations are underway to resolve some of these issues.

Finally, a comparison of fatigue crack growth characteristics between NiTi–TiC composites of this study and a representative Al–SiC metal–matrix composite is made. A large body of literature is available on such composites and has been reviewed [30,31] and a generalization of their fatigue behavior cannot be made given the often differing results. Results obtained on NiTi–TiC in this study are similar to those reported by Sugimura and Suresh [32], who have conducted fatigue crack growth experiments on peak-aged Al–3.5 wt.% Cu alloy reinforced with 6, 13, and 20 vol.% SiC particles. Their work shows that the addition of SiC particles increases the threshold for fatigue crack growth initiation (after accounting for the plasticity-induced crack closure) as compared to the unreinforced matrix material. However, within the composites with differing amounts of particles, no obvious relationship between the concentration of reinforcement particles and the rate of fatigue crack growth or the threshold is observed [32]. Furthermore, fractographic observations indicate that the primary failure process during fatigue fracture involves the fracture of SiC particles accompanied by ductile failure of the matrix. These observations in Ref. [32] are remarkably similar to those observed in this work, indicating that the micromechanisms of crack growth are similar in NiTi–TiC wherein the matrix deforms both through twinning and slip and Al–SiC wherein the matrix deforms only by slip. Even though twinning is an available mechanism for deformation it does not appear to dominate the behavior in the composites' response to fatigue.

5. Concluding remarks

Fatigue crack growth experiments were conducted on near-stoichiometric martensitic NiTi with and without TiC particle reinforcement. The overall response of the NiTi–TiC composites is similar to that of unreinforced NiTi, except for some subtle differences that are rationalized by recourse to fractography. The lack of significant fatigue differences is surprising since the uniaxial tensile stress–strain response of NiTi and NiTi–TiC are significantly different, with the composite showing lower ductility and higher twinning stresses. This could be due to a combination of factors such as microcracking, crack-deflection and the accommodation observed previously in shape-memory and superelastic composites [8,12,25]. Thus, the reinforcement concept can be used, for dilute concentrations at least, to tailor properties such as elastic modulus and transformation temperatures in NiTi without altering their fatigue crack growth characteristics.

Acknowledgements

The authors thank Professor S. Suresh (Massachusetts Institute of Technology) for the use of his mechanical testing facilities at the Laboratory for Experimental and Computational Micromechanics (LEXCOM) and for many helpful discussions. This work has also benefited from the use of the Los Alamos Neutron Science Center at the Los Alamos National Laboratory (LANL), funded by the US Department of Energy and operated by the University of California under Contract W-7405-ENG-36. RV and DCD acknowledge financial support from Daimler-Benz AG, Germany. Experimental help from Dr M.A.M. Bourke (LANL) and Mr G. LaBonte (LEXCOM) is also gratefully acknowledged.

References

[1] K. Otsuka, C.M. Wayman, Shape Memory Materials, Cambridge University Press, Cambridge, 1998.
[2] H. Funakubo, Shape Memory Alloys, Gordon and Breach, New York, 1987.
[3] D. Mari, D.C. Dunand, Metall. Mater. Trans. 26A (1995) 2833.
[4] D. Mari, L. Bataillard, D.C. Dunand, R. Gotthardt, J. Phys. IV 5 (1995) 659.
[5] K.L. Fukami-Ushiro, D.C. Dunand, Metall. Mater. Trans. 27A (1996) 183.
[6] K.L. Fukami-Ushiro, D. Mari, D.C. Dunand, Metall. Mater. Trans. 27A (1996) 193.
[7] D.C. Dunand, D. Mari, M.A.M. Bourke, J.A. Goldstone, J. Phys. IV 5 (1995) C8–653.
[8] D.C. Dunand, D. Mari, M.A.M. Bourke, J.A. Roberts, Metall. Mater. Trans. 27A (1996) 2820.
[9] K. Johansen, PhD Thesis, Ruhr-Universität, 1998.
[10] K. Johansen, H. Voggenreiter, G. Eggeler, Mater. Sci. Eng. A A273–275 (1999) 410.
[11] M.A.M. Bourke, J.A. Goldstone, T.M. Holden, in: M.T. Hutchings, A.D. Krawitz (Eds.), Measurement of Residual and Applied Stress using Neutron Diffraction, Kluwer Academic, Netherlands, 1992, p. 369.
[12] R. Vaidyanathan, M.A.M. Bourke, D.C. Dunand, Acta Mater. 47 (1999) 3353.
[13] T.M. Poletika, S.N. Kulkov, V.E. Panin, Poroshkovaya Metall. 7 (247) (1983) 560.
[14] S.N. Kulkov, T.M. Poletika, A.Y. Chukhlomin, V.E. Panin, Poroshkovaya Metall. 8 (260) (1984) 88.
[15] T.B. Massalski, Binary Alloy Phase Diagrams, vol. 1, 2nd edition, ASM, New York, 1987.
[16] H.J. Bunge, Texture Analysis in Materials Science, Butterworth-Heinemann, Guilford, UK, 1982.
[17] R. Vaidyanathan, M.A.M. Bourke, D.C. Dunand, J. Appl. Phys. 86 (1999) 3020.
[18] H.M. Rietveld, J. Appl. Crystallogr. 2 (1969) 65.
[19] A.C. Larson, R.B. VonDreele, General Structure Analysis System (GSAS), Report No. LAUR 8-748, Los Alamos National Laboratory, 1986.
[20] R.H. Dauskardt, T.W. Duerig, R.O. Ritchie, in: M. Doyama et al. (Eds.), Proc. of the MRS Intl. Mtg. on Adv. Mater., Vol. 9: Shape Memory Materials, Tokyo, Japan, Materials Research Society, Pittsburgh, PA, USA, 1989, p. 243.
[21] R.L. Holtz, K. Sadananda, M.A. Imam, in: R.J. Aresnault (Ed.), Proc. of The Johannes Weertman Symp, TMS, Warrendale, PA, 1996, p. 297.
[22] S. Suresh, Fatigue of Materials, Cambridge University Press, Cambridge, 1991.
[23] Y.C. Shu, K. Bhattacharya, Acta Mater. 46 (1998) 5457.
[24] M.A.M. Bourke, R. Vaidyanathan, D.C. Dunand, Appl. Phys. Lett. 69 (1996) 2477.
[25] R. Vaidyanathan, M.A.M. Bourke, D.C. Dunand, Mater. Sci. Eng. A273–275 (1999) 404.
[26] R. Vaidyanathan, Ph.D. Thesis, Massachusetts Institute of Technology (1998).
[27] K.N. Melton, O. Mercier, Acta Metall. 27 (1979) 137.
[28] S. Miyazaki, M. Suizu, K. Otsuka, T. Takshima, in: M. Doyama et al. (Eds.), Proc. of the MRS Intl. Mtg. on Adv. Mater., Vol. 9: Shape Memory Materials, Tokyo, Japan, Materials Research Society, Pittsburgh, PA, USA, 1989, p. 263.
[29] U. Ramamurty, Metall. Mater. Trans. A 30A (1999) 2237.
[30] J.E. Allison, J.W. Jones, in: S. Suresh, A. Mortensen, A. Needleman (Eds.), Fundamentals of Metal Matrix Composites, Butterworth-Heinemann, Guilford, UK, 1993, p. 269.
[31] J.J. Lewandowski, P.M. Singh, Metals Handbook, vol. 19, TMS, Warrendale, PA, 1996, p. 895.
[32] Y. Sugimura, S. Suresh, Metall. Trans. A 23A (1992) 2231.